Journal of Alloys and Compounds 488 (2009) 47–51

Contents lists available at ScienceDirect

Journal of Alloys and Compounds

journal homepage: www.elsevier.com/locate/jallcom

Microstructure and compressive properties of in situ synthesized Nd_2O_3/Ti–6Si (wt.%) alloy composites

Yongzhong Zhan*, Xinjiang Zhang, Guanghua Zhang, Honglou Mo

Laboratory of Nonferrous Metal Materials and New Processing Technology, Ministry of Education, Guangxi University, Nanning, Guangxi 530004, PR China

ARTICLE INFO

Article history:
Received 31 July 2009
Received in revised form 14 August 2009
Accepted 15 August 2009
Available online 22 August 2009

Keywords:
Metals and alloys
X-ray diffraction
Scanning electron microscopy

ABSTRACT

In situ Nd_2O_3/Ti–6Si (wt.%) alloy composites were synthesized utilizing the reaction from Ti, Si, Nd and SiO_2 through homogeneously melting in a non-consumable vacuum arc melting furnace. The XRD results show that the composites clearly contain α-Ti, β-Ti, Ti_5Si_3 and the in situ synthesized Nd_2O_3 reinforcements. The continuous and quasi-continuous network-shape Ti_5Si_3 + Ti eutectic cells abundantly exist, and Nd_2O_3 grows from near-equiaxed shape to dendritic shape with increase of Nd content in the composites. From the investigations on compressive properties of composites, it is deduced that the significant improvement in modulus and strength can be attributed to the presence of abundant Nd_2O_3 in the composites.

1. Introduction

Ti–Si alloys have been considered for potential high-temperature structural applications because of their physical, chemical and mechanical properties, such as high melting point, oxidation resistance and excellent specific strength [1–3]. As the reinforcement in Ti–Si alloys, the hard brittle phase Ti_5Si_3 compound with a complex $D8_8$ hexagonal structure (Mn_5Si_3-type, $a = 0.7444$ nm, $c = 0.5143$ nm) has high melting point, low density, good oxidation resistance and creep resistance. Therefore, this intermetallic can significantly improve the mechanical properties of the Ti–Si alloys [4–8].

In recent years, different in situ techniques have attracted more attention as a method to prepare discontinuous–reinforced titanium matrix composites (TMCs) because of the ease of fabrication, lower cost, and isotropic properties. Usually, self-propagation high-temperature synthesis (SHS) [9,10], powder metallurgy (PM) [11], mechanical alloying (MA) [12,13], rapid solidification powder processing (RSP) [14,15] and casting [16,17] have been used to produce titanium matrix composites by in situ processing techniques. The rare earth oxide (RE_2O_3) formed by in situ technique was proved to be valuable to increase the mechanical properties due to the fine size of the dispersion and their high thermal stability in the titanium matrix. For instance, Geng et al. [17,18] and Wang et al. [19] have reported that in situ synthesized RE_2O_3 reinforcements (La_2O_3, Y_2O_3 or Nd_2O_3) together with TiB particles, which were prepared by the common casting method, can significantly improve the tensile strength of titanium matrix composites.

In the present work, Nd_2O_3/Ti–6Si (wt.%) alloy composites were in situ synthesized utilizing the reaction between Ti, Si, Nd and SiO_2 through the following reaction:

$$4Nd + 3SiO_2 = 2Nd_2O_3 + 3Si \quad (1)$$

$$5Ti + 3Si = Ti_5Si_3 \quad (2)$$

In the composites, the phases and microstructure were examined, at the same time, the compressive properties at room temperature were studied and the fractography was discussed.

2. Experimental procedure

In synthesizing Nd_2O_3/Ti–6Si (wt.%) alloy composites, the raw materials were pure sponge titanium (>99.9%), pure Si (>99.9%), pure Nd (>99.9%) and SiO_2 powder (>99.9%). The weight percentage of the reactants and the theoretical weight percentage of the products were listed in Table 1. Stoichiometric amounts of raw materials were blended and melted in a non-consumable vacuum arc melting furnace. To minimize compositional segregation and inhomogeneity, the ingots were turned over and remelted six times.

The phase components of all specimens were analyzed by the X-ray diffraction (XRD) experiment on a Rigaku D/Max 2500 V diffractometer operated at 40 kV, 250 mA, employing Cu Kα radiation as filtered by a graphite monochromator. For the microstructural analysis, the metallographic samples were prepared using conventional grinding and mechanical polishing techniques. The polished samples were etched in an erodent with composition of HF:HNO_3:Water = 1:2:6 (ratio by volume). The optical images were obtained in the DMM-660C optical microscopy and the Hitachi S-3400 scanning electron microscope (SEM) equipped with energy dispersive X-ray analysis (EDX). Compression tests were performed on Instron 8801 axial servohydraulic dynamic testing system. The compression specimens with the size of 5 mm × 5 mm × 10 mm were cut from the buttons by electric discharge machining (EDM), and then deformed to failure at room temperature in air at an initial

* Corresponding author. Tel.: +86 771 3272311; fax: +86 771 3233530.
E-mail address: zyzmatres@yahoo.com.cn (Y. Zhan).

0925-8388/$ – see front matter © 2009 Elsevier B.V. All rights reserved.
doi:10.1016/j.jallcom.2009.08.071

Table 1
Compositions of in situ Nd_2O_3/Ti–6Si (wt.%) alloy composites.

Samples	Reactants (wt.%)				Reinforcement Nd_2O_3 (wt.%)
	Ti	Si	Nd	SiO_2	
1	94.0	6	0	0	0
2	84.6	4.148	8.574	2.678	10
3	81.78	3.592	11.146	3.482	13
4	78.96	3.036	13.718	4.286	16

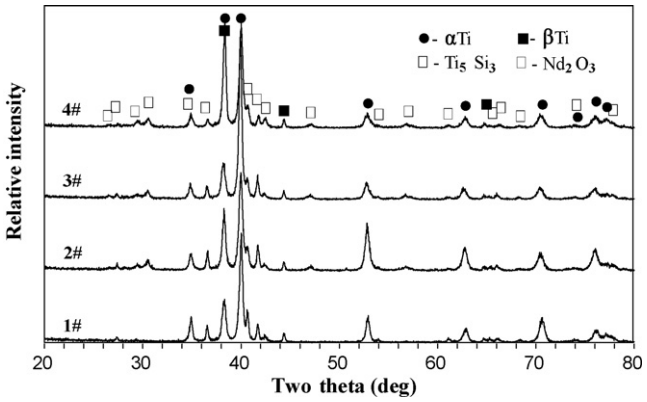

Fig. 1. X-ray diffraction patterns of all samples.

strain rate of 1 mm/min. Moreover, the fracture surfaces were characterized using scanning electron microscope (SEM).

3. Results and discussions

3.1. Microstructure

X-ray diffraction patterns of all samples are shown in Fig. 1. From the XRD pattern of sample 1, three different phases, namely α-Ti, Ti_5Si_3 and β-Ti, are found in the Ti–6Si alloy. However, the phase

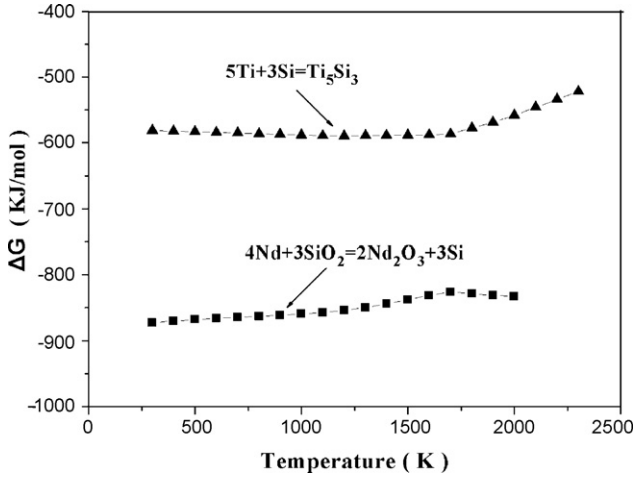

Fig. 2. The calculation results of Gibbs free energy (ΔG).

component of the other samples contains obviously α-Ti, Ti_5Si_3, β-Ti and Nd_2O_3. The results of the XRD analysis confirm that Ti–6Si alloy composites reinforced by in situ Nd_2O_3 particles can be synthesized utilizing the reaction between Ti, Si, Nd and SiO_2 during the melting process. The Gibbs free energy (ΔG) of reactions (1) and (2) has also been calculated by using the thermodynamic data from Ref. [20]. The result indicates that the Gibbs free energy of the two reactions is negative, so the formation of the Nd_2O_3 and Ti_5Si_3 phases directly from the reaction between Ti, Si, Nd and SiO_2 is favorable in thermodynamics, as is shown in Fig. 2.

Optical micrographs of the composites are presented in Fig. 3. In the microstructure of the sample 1 (Fig. 3a), Ti_5Si_3 particles distributed in the Ti matrix form the continuous and quasi-continuous network-shape eutectic cells. However, in the optical micrographs of the other samples, it is clearly shown that Nd_2O_3 reinforcements were in situ synthesized in the Ti–6Si alloy besides the Ti + Ti_5Si_3 eutectic cells, as is shown in Fig. 3b, c and d. In those compos-

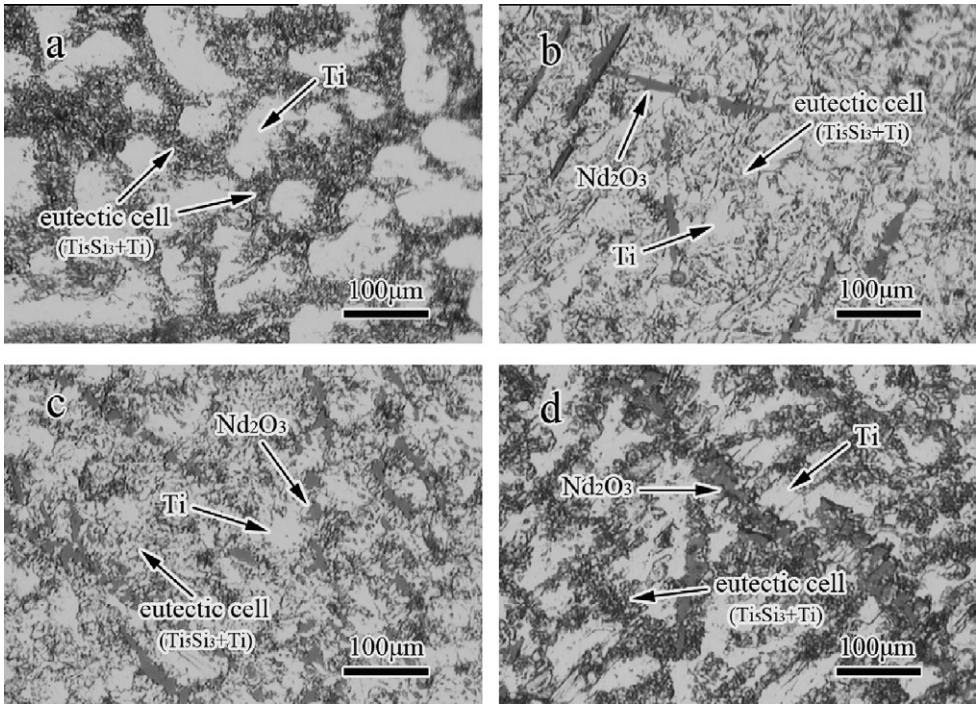

Fig. 3. Optical microstructures of all samples: (a) sample 1; (b) sample 2; (c) sample 3; (d) sample 4.

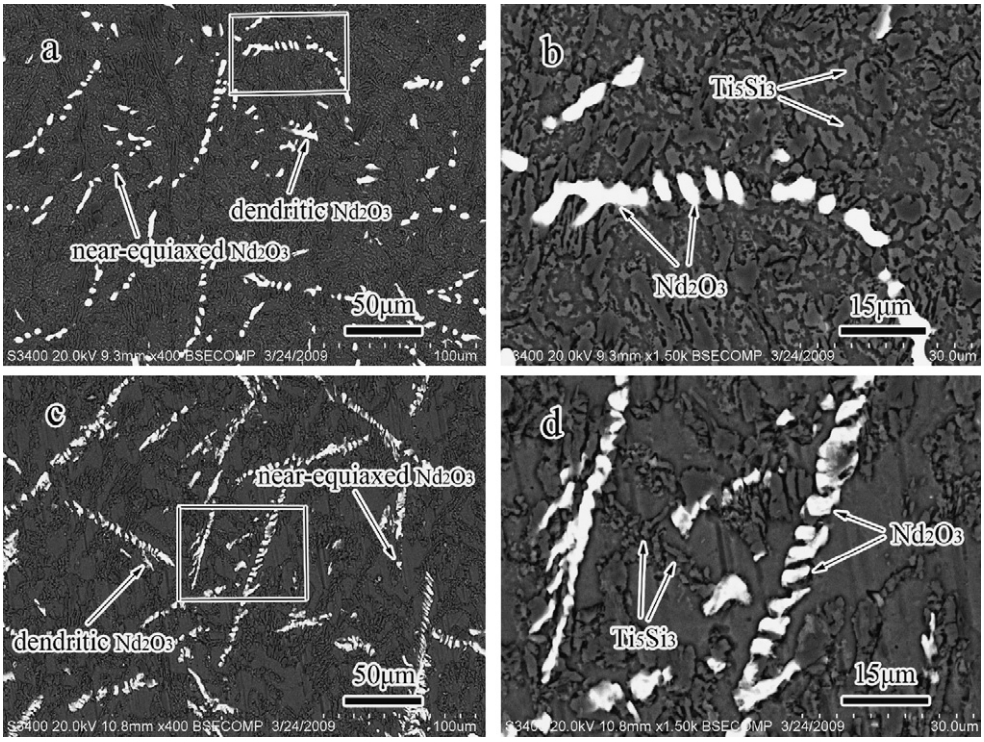

Fig. 4. SEM-BSE micrographs of the sample 2 and sample 4: (a) the morphologies and distribution of Nd_2O_3 reinforcements in the sample 2; (b) a magnified view of white boundary marked region in Fig. 3a; (c) the morphologies and distribution of Nd_2O_3 reinforcements in the sample 4; (d) a magnified view of white boundary marked region in Fig. 3c.

ites, the morphologies of the Nd_2O_3 reinforcements exhibit two shapes: dendritic and near-equiaxed shape. In order to distinguish the characteristics of Ti_5Si_3 and Nd_2O_3, the backscattered electron scanning microscopy was used to further examine the microstructure, as shown in Fig. 4. Since the atomic number of Nd (atomic number: 60) is much higher than those of Ti (atomic number: 22) and Si (atomic number: 14), Nd_2O_3 reinforcements exhibit more white in the backscattered SEM image. From Fig. 4, the dendritic and near-equiaxed shape Nd_2O_3 reinforcements were observed, at the same time, it can be seen that the abundant Ti_5Si_3 particles exist in the eutectic cell. Furthermore, the content of dendritic shape Nd_2O_3 reinforcement is increased when the weight percent of Nd_2O_3 increases.

The coarse primary RE_2O_3 particles can been formed due to the high addition amount of rare earth metals and the high chemical activity and the low melting point of pure rare earth metals [18,21,22]. In this work, the melting point of sponge titanium (1943 K) is higher than Nd (1283 K), so the rare earth metal Nd could melt before sponge titanium and react with oxygen resulting in formation of coarse primary Nd_2O_3 particles. Moreover, the weight percentage of Nd in the composites was more than 8.5 wt.%. In addition, when the melt cooled, Nd_2O_3 particles will precipitate first since Nd_2O_3 has a higher melting point (2272 °C) than Ti_5Si_3 (2130 °C). As a result, the solid Nd_2O_3 particles in the melt can supply heterogeneous nucleation sites for subsequent formation of the Ti_5Si_3 phases from the melt before the solidification of the matrix alloy.

3.2. Compressive properties

Fig. 5 shows the representative stress–strain curves of the compression behavior at room temperature for all the samples. Furthermore, the compressive properties including Young's modulus (E), ultimate compressive strength (UCS) and fracture strain (ε) of both Ti–6Si alloy and Nd_2O_3/Ti–6Si alloy composites tested at room temperature are shown in Table 2. The measurement errors are below 5%. According to Table 2, the Young's modulus (34,340–38,390 MPa) and ultimate compressive strength (1538–1607 MPa) of Nd_2O_3/Ti–6Si composites are significantly higher than that of Ti–6Si alloy (E: 29,110 MPa, UCS: 1436 MPa). However, the fracture strain of Nd_2O_3/Ti–6Si alloy composites is

Table 2
Compressive properties of each sample.

Samples	E (MPa)	UCS (MPa)	ε (%)
1	29,110	1436	22.02
2	38,390	1572	12.87
3	34,340	1607	13.35
4	35,770	1538	10.32

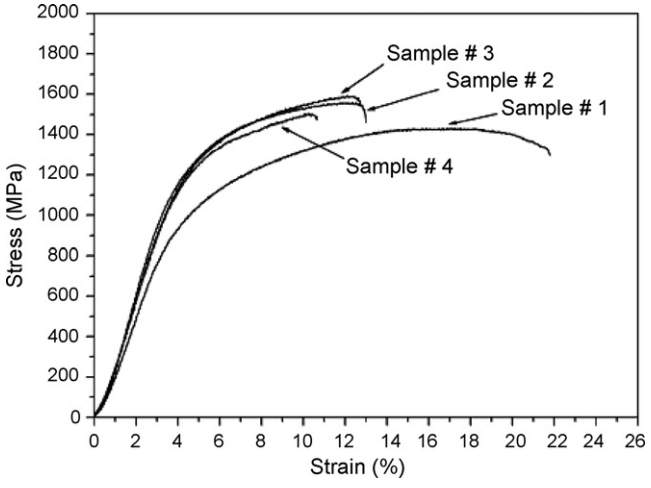

Fig. 5. Compression stress–strain curves of all the samples at room temperature.

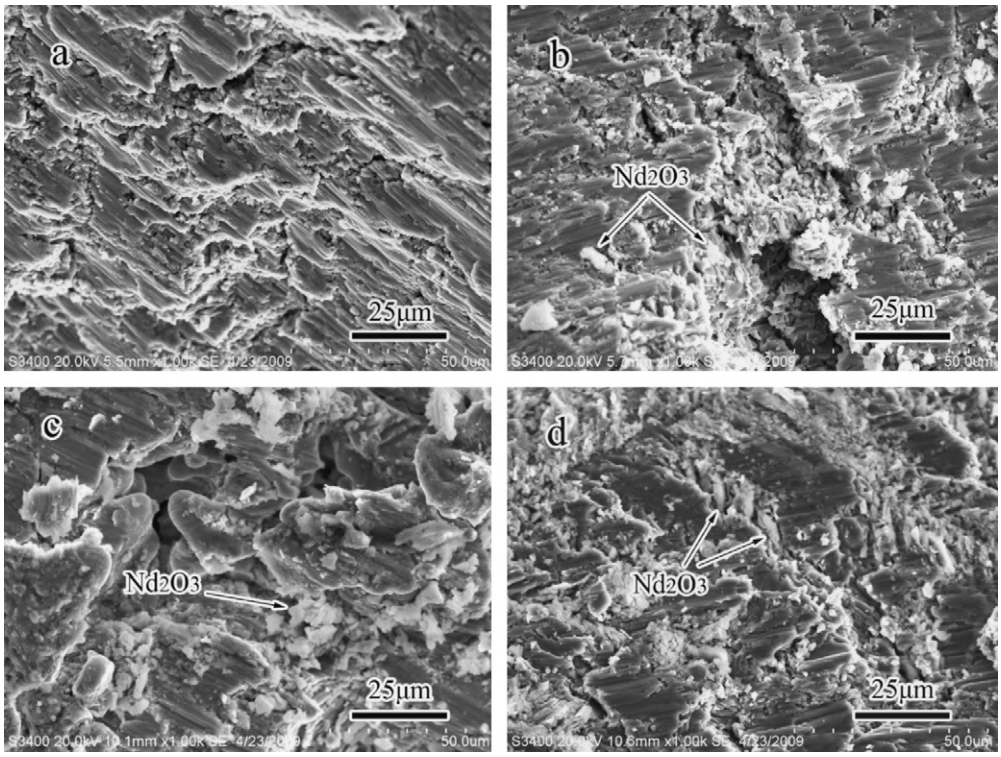

Fig. 6. SEM images of fractured surfaces for the compressive samples: (a) sample 1, (b) sample 2, (c) sample 3, (d) sample 4.

approximately reduced by 50%. It can be concluded that in situ synthesis of Nd_2O_3 reinforcements significantly increased the strength of Ti–6Si alloy, while the plasticity decreased correspondingly.

As is discussed above, the introduction of in situ Nd_2O_3 particles can significantly improve the compressive strength and Young's modulus of Ti–6Si alloy. Hard Nd_2O_3 and Ti_5Si_3 particles in the composites act as the obstacles to hinder the motion of dislocations. It is because that a dislocation passing into the near grains or dendrites of different orientations has to change its direction of motion. Meanwhile, the atomic disorder within a boundary region will result in a discontinuity of slip planes from one to the other. Furthermore, the interaction of different dislocation areas also contributes to the improvement of the compressive strength and Young's modulus. Consequently, the strengthening mechanisms of the composites may be mainly attributed to the load transfer from the soft matrix onto the hard reinforcements and dispersion strengthening from the finer Nd_2O_3 reinforcements.

According to Refs. [18,19,23], the strength of the particle–reinforced composites can usually be calculated approximately as:

$$\sigma \approx f_{Ti}\sigma_{Ti} + f_{Ti_5Si_3}\sigma_{Ti_5Si_3} + f_{Nd_2O_3}\sigma_{Nd_2O_3}$$

where f_{Ti}, $f_{Ti_5Si_3}$ and $f_{Nd_2O_3}$ are the contents of the titanium matrix, Ti_5Si_3 and Nd_2O_3, respectively, while σ_{Ti}, $\sigma_{Ti_5Si_3}$ and $\sigma_{Nd_2O_3}$ are the compressive strengths of the titanium matrix, Ti_5Si_3 and Nd_2O_3, respectively. It is well known that Nd_2O_3 is the hard ceramic particle, which has higher strength comparing with the soft titanium matrix. Therefore, the dispersed Nd_2O_3 ceramic particles improve the compressive strength of the Ti–6Si alloy.

Fig. 6 shows the typical SEM micrographs of the fractured surfaces for the compressive sample. All of the materials show the brittle cleavage fracture characteristic on a macroscopic scale. The fractured surface of Ti–6Si alloy shows smooth and flat surface, and the cleavage facet of Ti_5Si_3 particles and the tiny avulsion edges are shown in Fig. 6a. However, the Nd_2O_3/Ti–6Si alloy composites are characterized by coarse cleavage facets compared with that of Ti–6Si alloy, as is shown in Fig. 6b, c and d. Furthermore, some pulled out Nd_2O_3 particles are found on the fractured surface, where a crack propagates through the Ti_5Si_3/matrix interface. The cracked Nd_2O_3 particles were observed indicating that they could undertake load during compression test.

4. Conclusion

In situ Nd_2O_3/Ti–6Si (wt.%) alloy composites can been synthesized utilizing the reaction between Ti, Si, Nd and SiO_2 through homogeneously melting in a non-consumable vacuum arc melting furnace.

The reinforcements were homogeneously distributed in the composites. The continuous and quasi-continuous network-shape Ti_5Si_3 + Ti eutectic cell abundantly exist in those composites, and Nd_2O_3 grows from near-equiaxed shape to dendritic shape with increase of Nd content. The Nd_2O_3 particles in the melt can supply heterogeneous nucleation sites for subsequent formation of the Ti_5Si_3 phase from the melt, before the solidification of the matrix alloy.

The compressive strength and the Young's modulus of Nd_2O_3/Ti–6Si alloy composites are superior to those of Ti–6Si alloy. However, the ductility of the composites is decreased comparing with that of Ti–6Si alloy. The strengthening mechanisms of the composites can be mainly attributed to the undertaking load of the Nd_2O_3 reinforcements.

Acknowledgements

The authors wish to express thanks to the financial support from the National Natural Science Foundation of China (50761003), the Key Project of China Ministry of Education (207085) and the Opening Foundation of State Key Laboratory of Powder Metallurgy.

References

[1] Y.Z. Zhan, Z.W. Yu, Y. Wang, Y.F. Xu, X.B. Shi, Tribol. Lett. 26 (2007) 25.
[2] N. Zotov, D. Parlapanski, J. Mater. Sci. 29 (1994) 2813.
[3] D.M. Shah, D. Berczik, D.L. Alton, R. Hetcht, Mater. Sci. Eng. A 155 (1992) 45.
[4] Y.Z. Zhan, X.J. Zhang, J. Hu, Q.H. Guo, Y. Du, J. Alloy Compd. 479 (2009) 246.
[5] T. Sandwick, K. Rajan, J. Electron. Mater. 19 (1990) 1193.
[6] D.M. Shah, D. Berczik, D.L. Anton, R. Hecht, Mater. Sci. Eng. A 155 (1992) 45.
[7] A.N. Enyashin, A.L. Ivanovskii, Physica E 41 (2009) 1217.
[8] C.L. Yeh, C.C. Hsu, J. Alloy Compd. 395 (2005) 53.
[9] H.T. Tsang, C.G. Chao, C.Y. Ma, Scripta Mater. 37 (9) (1997) 1359.
[10] T. Yamamoto, A. Otsuki, K. Ishihara, P.H. Shingu, Mater. Sci. Eng. A 239/240 (1997) 647.
[11] B. Yang, E.L. Zhang, Y.X. Jin, Z.J. Zhu, S.Y. Zeng, J. Mater. Sci. Technol. 17 (2001) 103.
[12] L.L. Ye, Z.G. Liu, M.X. Quan, Z.Q. Hu, J. Appl. Phys. 80 (1996) 1910.
[13] L. Lu, M.O. Lai, H.Y. Wang, J. Mater. Sci. 35 (2000) 241.
[14] S. Rangarajan, P.B. Aswath, W.O. Soboyejo, Scripta Mater. 35 (1996) 239.
[15] S. Dubey, Y. Li, K. Reece, W.O. Soboyrjo, R.J. Lederich, Mater. Sci. Eng. A 266 (1999) 303.
[16] Y.G. Li, L. Xiao, W.J. Lu, J.N. Qin, D. Zhang, Mater. Sci. Eng. A 488 (2008) 415.
[17] K. Geng, W.J. Lu, D. Zhang, T. Sakata, H. Mori, Mater. Des. 24 (2003) 409.
[18] K. Geng, W.J. Lu, D. Zhang, Mater. Eng. A 360 (2003) 176.
[19] L.Q. Wang, W.J. Lu, J.N. Qin, F. Zhang, D. Zhang, Mater. Sci. Eng. C 29 (2009) 1897.
[20] O. Knacke, O. Kubascheswski, R. Hesselman, Thermochemical Properties of Inorganic Substance, 2nd ed., Springer-Verlag, Berlin, 2003, pp. 1180, 1190, 1480, 1505, 1519, 1666.
[21] Z.F. Yang, W.J. Lu, D. Xu, J.N. Qin, D. Zhang, J. Alloy Compd. 419 (2006) 76.
[22] Z.F. Yang, W.J. Lu, L. Zhao, J.Q. Lu, J.N. Qin, D. Zhang, Mater. Lett. 61 (2007) 2368.
[23] Z.F. Yang, W.J. Lu, J.N. Qin, D. Zhang, Mater. Sci. Eng. A 425 (2006) 185.